The 65-kDa carrot microtubule-associated protein forms regularly arranged filamentous cross-bridges between microtubules

Jordi Chan*, Cynthia G. Jensen†, Lawrence C. W. Jensen†, Max Bush*, and Clive W. Lloyd*‡

*Department of Cell Biology, John Innes Centre, Norwich NR4 7UH, United Kingdom; and †Department of Anatomy, University of Auckland, School of Medicine, Private Bag 92019, Auckland, New Zealand

Edited by Lewis G. Tilney, University of Pennsylvania, Philadelphia, PA, and approved November 1, 1999 (received for review July 9, 1999)

In plants, cortical microtubules (MTs) occur in characteristically parallel groups maintained up to one microtubule diameter apart by fine filamentous cross-bridges. However, none of the plant microtubule-associated proteins (MAPs) so far purified accounts for the observed separation between MTs in cells. We previously isolated from carrot cytoskeletons a MAP fraction including 120- and 65-kDa MAPs and have now separated the 65-kDa carrot MAP by sucrose density centrifugation. MAP65 does not induce tubulin polymerization but induces the formation of bundles of parallel MTs in a nucleotide-insensitive manner. The bundling effect is inhibited by porcine MAP2, but, unlike MAP2, MAP65 is heat-labile. In the electron microscope, MAP65 appears as filamentous cross-bridges, maintaining an intermicrotubule spacing of 25–30 nm. Microdensitometer-computer correlation analysis reveals that the cross-bridges are regularly spaced, showing a regular axial spacing that is compatible with a symmetrical helical superlattice for 13 protofilament MTs. Because MAP65 maintains *in vitro* the inter-MT spacing observed in plants and is shown to decorate cortical MTs, it is proposed that this MAP is important for the organization of the cortical array *in vivo*.

A distinctive feature of the cortical array in higher plants is the parallelism of the microtubules (MTs). Electron microscopy (EM) studies show that the array is composed of overlapping MTs that can maintain a parallel relationship over several micrometers (1, 2). Averaged over the entire cell, this degree of order allows the directionality of the entire array to be summarized as "one cell: one microtubule alignment" (3) that can be transverse to the cell's long axis or oblique or longitudinal. Immunofluorescence studies show that most cells have organized arrays, with only a few percent being random (3, 4). The factor responsible for this spacing is, therefore, an important element in contributing to the large-scale organization and integrity of the array (5). It is also likely to be involved in channeling the movement of the plasma membranous cellulose synthesizing particles (6).

At the EM level, MTs are commonly seen to occur in parallel groups interconnected by filamentous cross-bridges with lengths approximating the diameter of the MTs (1, 2, 7, 8). Several attempts have been made to isolate these filamentous microtubule-associated proteins (MAPs). Cyr and Palevitz (9) found that high speed supernatants from carrot suspension cells caused the bundling of MTs *in vitro*, with a center–center spacing of 34 nm. A maize MAP fraction containing a range of proteins that also causes MT bundling has been described (10). Jiang *et al.* (11) showed that a crude cytoplasmic extract from evacuolated tobacco protoplasts bundled MTs with cross-links of two different lengths: 20–25 and 12–15 nm. Later, Jiang and Sonobe (12) used this cytosolic extract to isolate a group of 65-kDa microtubule-associated proteins. Although these proteins induced bundling, they did not form the longer, 20- to 25-nm filamentous cross-bridges. Therefore, no protein has so far been isolated from plant cells that forms filamentous cross-bridges capable of spanning the intermicrotubule gap observed *in vivo*. In a previous paper, we (13) reported the isolation of a MAP fraction (including, among others, a 120-kDa polypeptide and a triplet at 60, 62, and 68 kDa—the so-called 65-kDa MAPs) from carrot cytoskeletons. Now, we have purified the 65-kDa MAPs, have characterized their MT bundling activity, and have demonstrated that they bind to MTs in a regular pattern, maintaining an inter-MT spacing consistent with the dimensions observed in cells. We suggest that the presence of MAP65 is sufficient to account for the characteristically parallel organization of the cortical MT array and is therefore likely to be important for plant morphogenesis.

Materials and Methods

Cells. Cells were maintained as described (14) except coconut milk was omitted. Four-day-old cells were protoplasted by using 2% (wt/vol) Onozuka R-10 cellulase (Yakult Pharmaceutical, Tokyo), 0.05% Pectolyase Y-23 (Yakult Pharmaceutical) in culture medium plus 0.04 M sorbitol. After 3 h, protoplasts were washed and collected in PEM buffer (50 mM Pipes, pH6.9/5 mM EGTA/5 mM $MgSO_4$) plus 0.4 M sorbitol.

Isolation of Proteins. Triton X-100-extracted cytoskeletons were prepared according to the adaptation of the method of Hussey *et al.* (15) by Xu *et al.* (16). Cytoskeletons were extracted in 2 vol of ice-cold 5 mM imidazole buffer (pH 7.5) containing 3 mM calcium and protease inhibitors. After 1 h on ice, the supernatant was collected at 55,000 × *g* for 30 min at 4°C, was filtered, and was stored in liquid nitrogen. Porcine brain tubulin was isolated essentially according to ref. 17 with three cycles of assembly/disassembly. Tubulin and MAPs were separated on DEAE-A50. Modifications included the use of 10% (vol/vol) DMSO instead of glycerol and the desalting of the tubulin by another round of assembly, concentrating the tubulin to 20–30 mg/ml.

Co-Sedimentation of Carrot Proteins on Porcine Taxol-MTs and Isolation of MAP65. MAP fractions were cleared by adding EGTA to 10 mM, plus protease inhibitors, then centrifuging at 85,000 × *g* for 40 min at 4°C. The supernatant was made to 20 μm of taxol, then 0.5 mg/ml taxol-stabilized porcine brain MTs were added. After 40 min on ice, the suspension was underlaid with 40% (wt/vol) sucrose in PEM plus 20 μm of taxol and was centrifuged at 65,000 × *g* for 30 min at 4°C. Pellets were rinsed twice in PEM-taxol, then were resuspended in a minimal volume of 500 mM NaCl in PEM-taxol plus protease inhibitors. The salt-eluted MAP fraction was diluted to bring the NaCl to 125 mM, then was concentrated on an Amicon Microcon 10 ultrafiltration unit. The protein concentrate was sedimented on a 4.5–27% sucrose

This paper was submitted directly (Track II) to the PNAS office.

Abbreviations: EM, electron microscopy; MAP, microtubule-associated protein; MT, microtubule; pf, protofilament.

‡To whom reprint requests should be addressed. E-mail: clive.lloyd@bbsrc.ac.uk.

density gradient for 15 h, 150,000 × *g*, 4°C, and MAP65-rich fractions were pooled.

Interactions of MAP65 with MTs. Tubulin was conjugated to rhodamine according to ref. 18. Rhodamine-MTs were put through another round of assembly/disassembly in 10% (vol/vol) DMSO and were stored in liquid nitrogen. To see whether MAP65 stimulated the self-assembly of tubulin, it was added to non self-assembling concentrations of ρ-tubulin, which could be induced to assemble by high molecular weight, heat-stable porcine MAPs. To test its heat stability, MAP65 was placed in boiling water for 2 min, then on ice. For bundling assays, rhodamine-tubulin at 0.1 μg/μl was polymerized by adding 5 μM taxol and 5% (vol/vol) DMSO. All nucleotides were added at 2 mM. In other experiments, NaCl was added at 0–1 M to see whether it would dissociate preformed bundles. After 30 min at 37°C, the reaction was stopped with 9 vol of 1% (vol/vol) glutaraldehyde. The contrast/brightness of confocal microscope images of bundled fluorescent MTs was adjusted by using ADOBE PHOTOSHOP 4 (Adobe Systems, Mountain View, CA). To obtain a semiquantitative estimation of MT bundling, we first counted apparently single fluorescent MTs in tubulin-only controls, taking large, randomly selected fields of view to produce a mean. We then subtracted from this the mean figure obtained from the MAP65 sample, taking the difference to represent the number of MTs in bundles. This was then converted to a percentage. Because single MTs cannot be resolved by fluorescence microscopy, we examined samples by negative staining in the EM; this confirmed that what appeared as single MTs by fluorescence were overwhelmingly single in the EM.

Acquisition and Analysis of EM Data. For EM studies, MAP65 was added to unlabeled tubulin in 5% DMSO/5 μM taxol in PEM. Samples were fixed in 2% glutaraldehyde/2% tannic acid in PEM. MT pellets were postfixed in 1% (vol/vol) osmium tetroxide, were dehydrated in an ethanol series, and were embedded in LR White acrylic resin. Silver sections (60–90 nm) were placed on pyroxylin and carbon-coated grids, were stained with uranyl acetate and lead citrate, and were photographed with a JEOL 1200EX electron microscope. From nine EM negatives with original magnifications of ×39,200, areas were selected between two parallel MTs corresponding on the original sections to lengths between 220 and 445 nm. Care was taken to avoid areas in which MTs lay on top of each other. Positive transparencies of each area were printed at final magnifications of ×117,600. The technique of microdensitometer-computer analysis has been described in detail elsewhere (19). In brief, the transparencies were scanned with a microdensitometer and were digitized by using a BBC Master computer (Acorn Computers, Cambridge, U.K.). Standard frequency domain filtering techniques were used to attenuate rapid density variations in the digitized densitometric record and to remove baseline drift caused by spatial variation of contrast in the micrograph. The filtered densitometer records were then converted to a binary data sequence representing the position of MT bridges on the original micrographs. Autocorrelograms of filtered data were obtained by correlating the complete data set with a shifted template consisting of either the first half or the second half of the record. With a Gamma PC computer (Gamma Computers, Auckland, New Zealand), the filtered densitometer records were cross-correlated with model templates, which were either single linear repeats between 16 and 40 nm or a series of symmetrical helical superlattices related to an underlying MT lattice composed of 13 protofilaments (pfs). These model templates have previously been proposed on the basis of biochemical and morphological data (19–21). A scaling of 90–110% of nominal length was used to obtain the best fit. To establish confidence levels, the correlation indices for the experimental data were compared with those for similar randomly generated data that had been correlated with the same model templates, also scaled to obtain the best fit. For a group of scans showing a single linear repeat, the optimal match was determined by obtaining the means of the scaled distances that provided the best fit for each scan. The overall mean significance level was determined for a complete set of records. To determine the number of pfs in the MT samples, transverse profiles of MTs printed at ×350,000 were scanned with a Microtek flatbed scanner (Microtek International, Hsinchu, Taiwan) attached to a Macintosh 7100 computer. A path was drawn around the middle of the wall of the MT, and a densitometer plot was obtained and was printed on a straight axis. The number of regularly spaced peaks that corresponded to the less-dense areas of the MT wall, representing the center of each pf, were counted. The diameter of MTs was measured from micrographs of MTs in transverse and longitudinal section and was correlated with the predetermined pf numbers. The relationship between MT diameter in longitudinal section and pf number was confirmed by comparison with previously published data on MT diameter and pf number (22, 23).

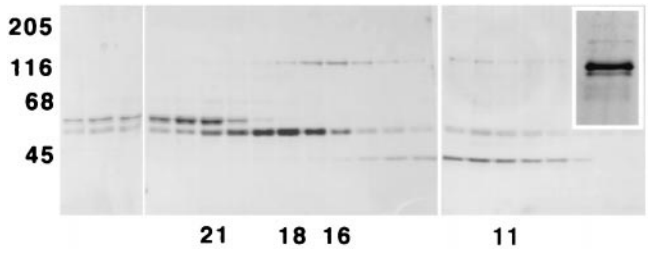

Fig. 1. Purification of MAP65. The carrot MAP fraction was purified by sucrose density centrifugation. The silver-stained gel of the fractions (28–5) shows separation of MAP65 from MAP120. Vertical axis, molecular weight markers; horizontal axis, key fractions. (*Inset*) Pooled MAP65 fraction showing the predominant 62-kDa member of the MAP65 triplet; MAP68 is shown as the thin band above.

Immunofluorescent Staining of MAP65 on Cortical MTs. To demonstrate that MAP65 decorates cortical MTs, substrate-attached disks of plasma membrane ("footprints") were prepared by settling carrot protoplasts onto poly-L-lysine-coated glass slides and then shearing them open by placing another slide on top. This exposed membrane-associated MTs, which were then stained by incubating in monospecific anti-MAP65 antibodies, as described in ref. 13, then with FITC-conjugated secondary antibodies.

Results

Purification of MAP65. MAP65 was isolated by sucrose-density gradient centrifugation from carrot MAP-fractions. Optimum results were from MAP fractions prepared by cosedimenting the cytoskeleton extract with porcine brain MTs in the presence of 70 mM NaCl. Fig. 1 shows that MAP65 consistently peaked in fractions 20–21 (sedimentation coefficient, 2.8S), whereas tubulin peaked in fraction 18 (4.7S), and MAP120 (6.6S) peaked in fraction 16. In different preparations, the MAP65 peak was always composed of the three MAP65 species: 60, 62, and 68 kDa. The MAP65 fractions were then pooled to assay function. Quantitative gel densitometry of the pool (Fig. 1 *Inset*) showed that the 60- to 62-kDa doublet was 89% of the total protein (in individual preparations, the 60-kDa species was always the minor polypeptide, being at least 4× less abundant than the 62-kDa species). The 68-kDa protein was 1.7% of the total pooled protein, and the 55-kDa tubulin doublet was 4.3%. The compe-

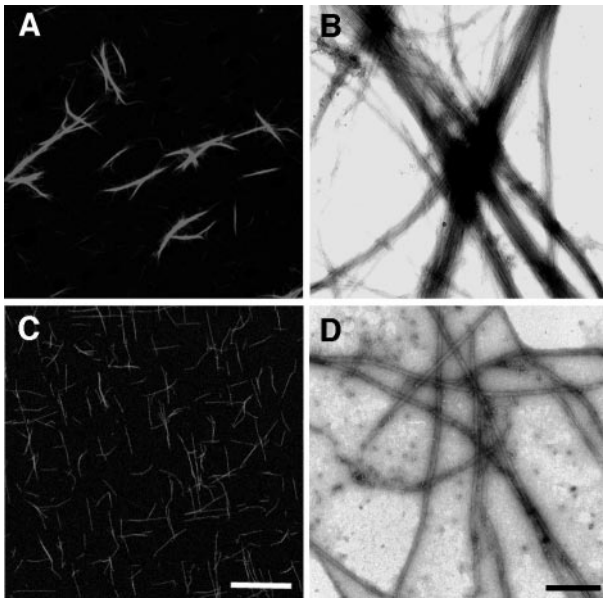

Fig. 2. MAP65 bundles microtubules. (*A*) Rhodamine-conjugated, taxol-stabilized MTs bundled by MAP65. (*B*) Negatively stained EM sample showing parallel, bundled MTs. (*C* and *D*) Control MTs without MAP65. [Bar = 36 μm (fluorescent images) and 500 nm (EM).]

tence of this preparation to bind MTs was confirmed in spin-down experiments.

MAP65 Induces the Bundling of Taxol-Polymerized Rhodamine-Labeled MTs. To investigate bundling effects, fractions from the sucrose gradient were mixed with 0.1 μg/μl rhodamine-labeled tubulin and 5 μM taxol to promote tubulin assembly. The peak MAP65 fractions promoted formation of thick bundles of parallel MTs, as seen by fluorescence microscopy (Fig. 2*A*). To confirm the nature of this bundling and to resolve individual MTs, samples were then negatively stained and were examined in the EM (Fig. 2*B*). In the absence of MAP65, MTs appeared to remain unbundled at the light microscope level (Fig. 2*C*). By negative staining, these unbundled MTs could be seen to be single (Fig. 2*D*). This assay was then used to investigate the bundling activity of other key fractions of the sucrose density gradient. Neither the tubulin peak nor the well separated p45 peak induced bundling (not shown). MAP120 did induce a low level of MT clustering, but this low level activity resulted in the formation of loose aggregates that were distinctly different from the characteristically tight bundles induced by MAP65.

These effects of MAP65 were concentration-dependent. This is illustrated in Fig. 3, which shows the MT bundling activity of MAP65 from 0.17–12 ng/μl. It will be seen that maximal activity was obtained above 8.5 ng/μl (0.1 μM). At this concentration, the addition of more MAP65 resulted in little difference to the mean percentage of bundled MTs, which remained at 80–90% of the available MTs, suggesting that it had reached saturation. In terms of molar ratio, this concentration corresponded to a MAP:tubulin dimer ration of 1:9. This suggests that the effects of MAP65 occur at substoichiometric ratios.

Bundling activity was insensitive to the addition of 2 mM ATP, GTP, AMP-PNP, or GMP-PNP. MAP65 heated in boiling water for 2 min had no bundling activity. The bundling effect of MAP65 was only seen either when tubulin was above the critical concentration or when taxol was added. To show that the bundling effect was independent of the presence of taxol, self-assembling concentrations of rhodamine-labeled tubulin were polymerized at 37°C; addition of carrot MAP65 then induced bundling in the absence of taxol.

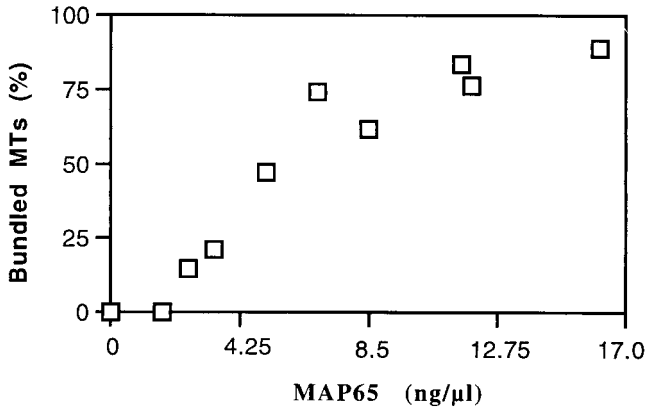

Fig. 3. Concentration effects of MAP65 on MT bundling. Increasing concentrations of MAP65 from 0 to 2 μM stimulate increased MT bundling (measured as percentage of single MTs relative to the MAP-free MT control).

Dissociation of bundles was only observed at 300 mM NaCl and above. These dissociated MTs had a mean length of 3.4 μm (0.14 SE, $n = 100$), which was at least 4× shorter than the mean length of intact MT bundles (14.6 μm, 0.82 SE, $n = 51$).

Effects of MAP65 on Tubulin Polymerization *in Vitro*. The ratio of tubulin:MAP65 was varied to investigate whether MAP65 induced polymerization of tubulin. By using non-self-assembling concentrations of rhodamine-tubulin [in PEM plus 5% (vol/vol) DMSO for 30 min at 37°C], MAP65 was added at molar ratios (to tubulin) ranging from 1:45 up to 1:1 but had no effect in inducing MT assembly. That subcritical concentrations of rhodamine-tubulin could be induced to assemble under these conditions was confirmed by adding high molecular weight, heat-stable porcine MAPs (MAP2 fraction). Such MTs, precoated with porcine MAPs, could not subsequently be induced to form bundles when carrot MAP65 was added. Immunoblots of supernatant and pellet from MT spin-down experiments confirmed that porcine MAP2 inhibited the binding of MAP65 to MTs (not shown).

MAP65 Forms Filamentous Projections Between Adjacent Parallel MTs. Thin sections of bundled MTs were examined by EM and, to ensure MTs that were extensively bundled, unlabeled tubulin was used at a molar ratio to MAP65 of 1:5. Thin sections of MAP65-MT pellets revealed the presence of filamentous projections interconnecting bundles of 2–10 parallel MTs (Fig. 4 *A*, *B*, *D*, *E*, and *G*). From 197 measurements (from 17 different MTs), the cross-bridges were found to have similar lengths, the majority peaking at 25–30 nm (Fig. 4*C*). The angle of projection was usually between 55 and 65°, giving the bundled MTs a "herringbone" appearance (Fig. 4*A*). No filaments were seen projecting free from a single MT. To determine whether the distribution of bridges was nonrandom, microdensitometer-computer correlation analysis was carried out on 26 selected areas between parallel MTs. This was cross-correlated with various model templates and showed marginally significant matches to the 12-dimer superlattice, 34- and 40-nm repeat templates [overall mean confidence levels of 93.8, 94.8, and 94.5% respectively (Table 1)]. Autocorrelograms derived from the filtered data were of two types. Fifteen scans showed a single repeat ranging from 34.7 to 37.8 nm (Fig. 4*F*), with highly significant ($P < 0.05$) matches to both 34- and 40-nm templates (in each case scaled to 36.9 ± 1.0 nm) (Table 1). The remaining

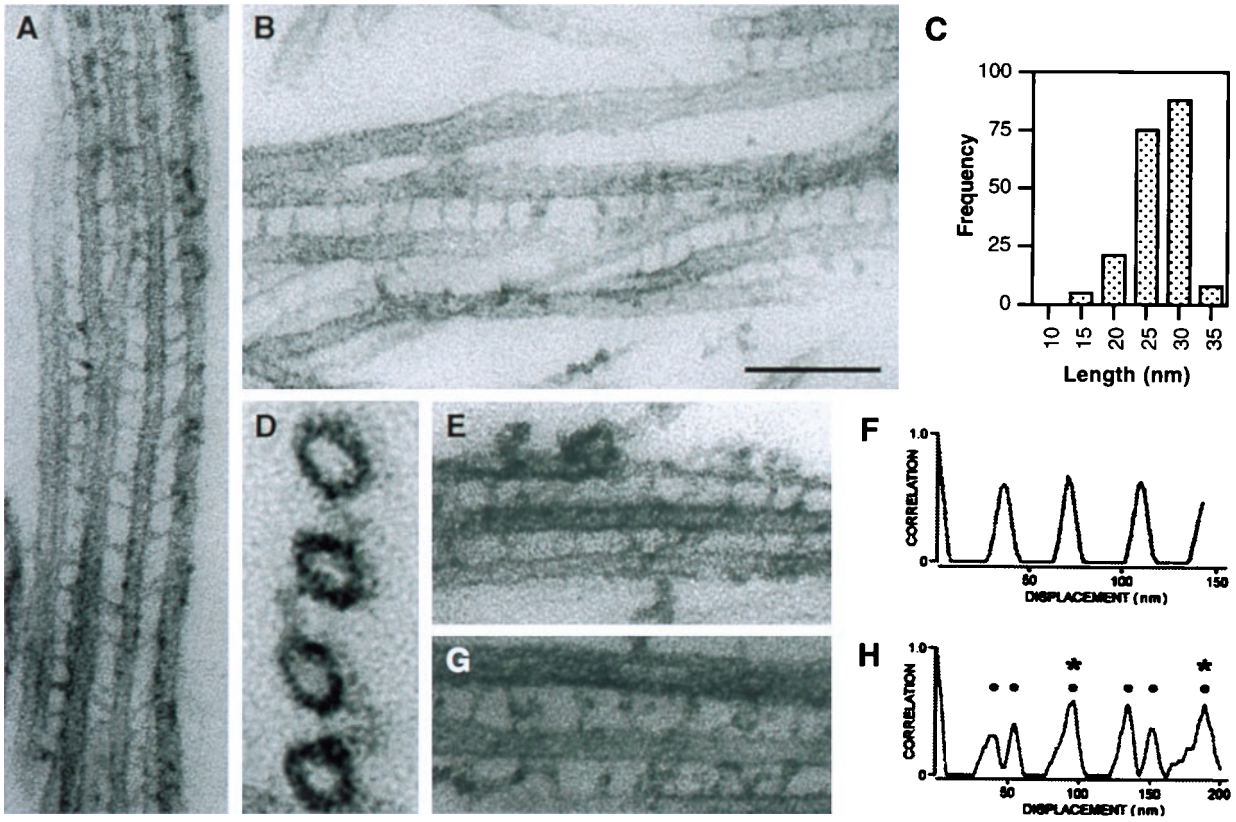

Fig. 4. (*A* and *B*) MTs bundled by MAP65. Inter-MT bridges appear as filaments projecting between walls of the MTs cut in longitudinal section. (*C*) Frequency histogram of the lengths of inter-MT bridges, which peak at 25–30 nm ($n = 197$). (*D*) MTs cut in transverse section, with filamentous bridges joining them. (*E*) The area between the upper two MTs was scanned to produce the autocorrelogram in *F*; a single axial repeat of 35.7 nm is evident. (*G*) The area between the upper two MTs was scanned to produce the autocorrelogram shown in *H*; peaks correspond to the spacings predicted by the 12-dimer superlattice model, which are indicated by dots. The lattice repeat distance is represented by strong peaks at 96 and 192 nm (asterisks). [Bar = 130 nm (*A*, *B*, *D*, *E* and *G*).]

11 most frequently showed spacings predicted by a superlattice model (Fig. 4*H*), with a highly significant match (overall mean confidence level of 99.7%; $P < 0.05$) to the 12-dimer superlattice template (Table 1).

We next tested whether these different patterns of decoration correlated with variable MT protofilament numbers. It was possible to determine the pf number of several MT profiles and to correlate this with MT diameter in transverse and longitudinal section. These data corresponded extremely well with previous correlations between pf number and MT diameter [Fig. 6 in Andreu *et al.* (22) and Figs. 5 and 6 in Jensen *et al.* (23)]. Of these MTs, 52% had diameters consistent with 12 pfs, 26% of the MTs with 13 pfs, and the remaining 26% with 11- and 14-pf MTs. The scans associated with the 12- and 13-pf MTs were analyzed further. Scans from 12-pf MTs showed a significant match (overall mean confidence level of 95.5%; $P < 0.05$) only to the 34-nm axial repeat template whereas scans associated with the 13-pf MTs showed a significant match (overall mean confidence level of 98.9%; $P < 0.05$) only to the 12-dimer superlattice template.

Table 1. Correspondence of MAP65 densitometer data to model templates

	Overall mean confidence level, %*		
Model	All files	Single repeat correlograms	Dimer correlograms
6-dimer	70.7	59.6	85.5
7-dimer	63.8	63.8	63.2
9-dimer	<50	55.5	<50
11-dimer	72.7	74.3	72.4
12-dimer	93.8	78.6	99.7
14-dimer	88.8	86.1	89.8
15-dimer	90.1	93.5	85.7
17-dimer	74.4	73.6	82.9
16-nm repeat	65.4	63.5	73.0
20-nm repeat	82.1	79.0	89.0
24-nm repeat	66.8	65.4	66.2
28-nm repeat	72.1	79.8	65.1
34-nm repeat	94.8	98.4	85.9
40-nm repeat	94.5	98.4	85.9

*Values of 95% and greater are considered significant ($P < 0.05$).

MAP65 Decorates Cortical MTs on Plasma Membrane Disks. Substrate-attached disks of plasma membrane, torn out of carrot protoplasts, contain cortical MTs still associated with the membrane. Fig. 5*A* shows such MTs stained with antibodies prepared by blot-affinity purification against the 65-kDa polypeptides. Compared with the anti-tubulin control (Fig. 5*B*), the staining is punctate, less continuous. This makes the point that the proteins that bundle brain MTs *in vitro* are located on plant cortical MTs *in vivo*.

Discussion

In Chan *et al.* (13), we found that a MAP fraction containing carrot MAP 120, MAP65, and other proteins caused the loose clustering of taxol-MTs. By separating the MAPs by sucrose density gradient centrifugation, it is now evident that MAP65

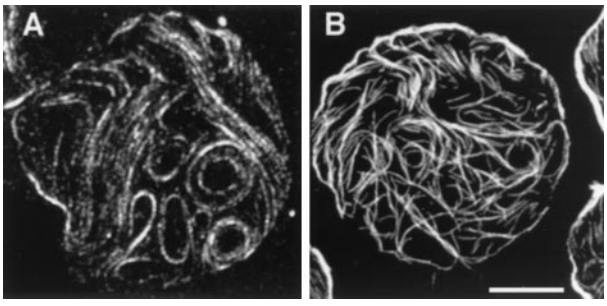

Fig. 5. Cortical MTs exposed on substrate-attached disks of plasma membrane from carrot protoplasts. Anti-MAP65 antibodies immunofluorescently stain the MTs in a punctate fashion (*A*), in contrast to the continuous pattern obtained with anti-tubulin (*B*). (Bar = 16 μm.)

possesses the ability to induce taxol-MTs to form bundles in which the parallel MTs are separated by filamentous projections.

Cyr and Palevitz (9) made the first steps toward identifying carrot MT-bundling proteins: they found that a mixture of proteins between 39 and 114 kDa formed bundles in which MTs were separated by 34 nm. Jiang *et al.* (11) also found that a crude homogenate of evacuolated protoplasts from tobacco BY-2 cells formed bridge-like structures. Later, Jiang and Sonobe (12) used MT affinity to isolate a group of ≈65-kDa proteins from such homogenates, but these purified MAPs were unable to form the longer 20- to 25-nm cross-bridges previously reported for the homogenate, and so it was concluded that "the 65 kDa protein . . . did not form the longer type of cross-bridge" (ref. 12, p. 899). However, our present data indicate that the MAP65 fraction does form long cross-bridges.

In our previous study (13), we prepared monospecific antibodies to the 68-kDa protein and showed that they immunoblotted the 60- as well as the 62-kDa bands; conversely, antibodies to the 60/62-kDa doublet recognized the 68-kDa band, indicating that the three polypeptides are antigenically related, and for this reason the are referred to as the "MAP65 family." In a subsequent study, we were unable to detect bundling with the 60-kDa polypeptide, which we purified by anion exchange chromatography (24). It could have become inactivated, but the possibility has to be considered that MAP65 isoforms differ in their ability to bundle MTs as is known for the neuronal MAP, tau (25). In the present study, MAP68 was virtually undetectable in the MAP65 fraction, which was found by quantitative densitometry to be 90% comprised of MAP62 and MAP60. Of these two polypeptides, MAP62 outweighed MAP60 by 4:1, and it is therefore probable that MAP62 is responsible for the observed activity. Other plant proteins, such as elongation factor 1α (26) and initiation factor (iso)4F (27), have also been reported to bundle MTs, but they do not form long cross-bridges.

Although the 65-kDa MAPs that form these projections are, like the structural brain MAPs, filamentous, there are significant differences. For example, MAP2 and tau are heat-stable whereas carrot MAP65 is not. Brain MAP2 was able to stimulate polymerization of neurotubulin under our conditions, but, despite repeated attempts, we were unable to demonstrate this for MAP65, even at high ratios relative to tubulin. This suggests that the properties of bundling and nucleation are separate, consistent with experiments showing that some constructs of tau can have a strong effect on bundling but a weak effect on nucleation (28). The major difference was that MAP65 could be readily seen to induce the bundling of taxol-MTs on the microscope slide whereas brain MAP2 could not. Overexpression of MAP2 in non-neuronal animal cells does cause MT bundling, but MAP2 does not seem to cause MTs to bundle readily *in vitro* (29, 30). How MAPs induce MT bundling is controversial (31). One idea (see refs. 27–30) is that MAPs stabilize MTs, reducing the electrostatic repulsion, allowing them to pack together. In this case, the projection domain of MAPs [or of other as yet unidentified animal proteins (31)] would then act as a passive spacer. An alternative view, that MAPs are active cross-linkers, seems more consistent with the ability of MAP65 to induce spontaneous bundling of MTs on the microscope slide without the need to pack them by centrifugation. This is unlikely to have been a side effect of primary stabilization because the MTs were already stabilized by taxol and MAP-free taxol-MTs never displayed spontaneous bundling. Accordingly, we suggest that the active MAP65 is a cross-linker, a possibility supported by the regularity of the structures formed.

It is interesting that the MAP65 bridges showed two different arrangements: a superlattice arrangement and a 34-nm axial repeat. This may be related to the variable pf number in taxol MTs (22) as our measurements indicate a mixture of 12- and 13-pf MTs. The superlattice arrangement of MAP65 bridges appears to be associated with the 13-pf MTs. This pf number occurs *in vivo* (32), and unpublished observations (C.G.J. and L.C.W.J.) indicate similar superlattice arrangements for plant cortical MTs. We therefore suggest that the arrangement for MAP65 is a 12-dimer superlattice when it associates with 13-pf MTs, both *in vitro* and *in vivo*. A 12-dimer superlattice arrangement is also characteristic of MAP2 and of inter-MT bridges from a variety of sources (19–21, 23). This might indicate common features of MAP decoration, and it is notable that MAP2 inhibited the bundling effect of carrot MAP65.

On the other hand, we find a single axial repeat arrangement for MAP65 bridges associated with 12-pf MTs. The lattice structure of 12-pf MTs may prevent MAP65 from binding in a superlattice. Although the 3-start helix surface lattice formed by the subunits appears to be highly conserved in MTs with different numbers of pfs (including 12), different pf numbers appear to be accommodated by a differential skewing of the pfs (see refs. 22 and 33–35 and references therein). This skewing of the pfs, as well as discontinuities in the surface lattice of 12-pf MTs, may prevent MAP65 from binding to 12-pf MTs in a 12-dimer helical superlattice and result instead in its binding along a single pf in a periodic fashion (33, 35). Single axial repeats such as this have also been found for the arrangement of the inter-MT bridges of foraminiferan protists (21).

The previous immunofluorescent staining of all four MT arrays (13) indicated that the 65-kDa MAP family is likely to function around the cell cycle, perhaps fulfilling variations of their bundling (or other) function(s) according to the stage of the cycle and the pattern of expression. However, the present investigations were performed with MAP fractions isolated from cultures overwhelmingly containing the interphase array (>95%), and for this reason we focus on the implications of the presence of a bundling proteins on cortical MTs. We have shown that MAP65 decorates exposed plasma membrane-associated MTs in a punctate fashion and is therefore highly likely to be responsible for maintaining the spacing between groups of parallel MTs *in vivo*. In living plant epidermal cells microinjected with rhodamine-tubulin, we have observed MT reorientation (36). This is a process whereby MTs convert between transverse and longitudinal configurations—a process implicated in the hormonally and environmentally controlled switching of the direction of cell expansion. After going through a mixed stage in which MTs of differing orientation coexist, cortical MTs become reorganized in parallel groups in the new direction. In view of the present results, we hypothesize that this parallelization, or "smoothing," involves the bringing of adjacent MTs into register by MAP65—the progressive "zipping-up" of local groups of MTs eventually super-adding to maintain overall uniformity of the array. It will be important to determine how the bundling

effect is modulated as the array switches between transverse and longitudinal orientations.

Cellulose microfibrils in the cell wall generally match the alignment of the underlying cortical MTs. To account for this, it has been hypothesized (see ref. 6 for review of models) that MTs impose channels on the plasma membrane to which they are attached and that rosettes of cellulose-synthesizing particles move within these fluid channels. In helping to bring MTs together, MAP65 would have a general influence on the path of the synthesizing particles. One general version of this could be that MAP65 only sporadically brings MTs together, leaving sufficiently wide lanes along which the synthases can travel. A more restricting version is conceivable: synthesizing particles could be railroaded into running between pairs of MTs whose parallelism is maintained by "ties" or "sleepers" formed by MAP65 cross-links. We note that the length of the 25- to 30-nm MAP65 inter-MT bridges creates sufficient distance to accommodate the diameter of the ≈24-nm (37) particle rosettes.

We thank Brian Wells for assistance with EM, Dr. A. Young and M. Watson for computer assistance, Oliver Ives for biochemical assistance, and Dr. Grant Calder for assistance with confocal microscopy. This work was funded by the Biotechnology and Biological Sciences Research Council (BBSRC) by way of a grant-in-aid to the John Innes Centre, and by a linked research grant between C.W.L. and the late Dr. R. Warn at the University of East Anglia.

1. Hardham, A. R. & Gunning, B. E. S. (1978) *J. Cell Biol.* **77,** 14–34.
2. Seagull, R. W. & Heath, I. B. (1980) *Protoplasma* **103,** 205–229.
3. Akashi, T. & Shibaoka, H. (1987) *Plant Cell Physiol.* **28,** 339–348.
4. Duckett, C. M. & Lloyd, C. W. (1994) *Plant J.* **5,** 363–372.
5. Lloyd, C. W. (1994) *Mol. Biol. Cell* **5,** 1277–1280.
6. Giddings, T. H. & Staehelin, L. A. (1991) in *The Cytoskeletal Basis of Plant Growth and Form*, ed. Lloyd, C. W. (Academic, London), pp. 85–99.
7. Lancelle, S. A., Callaham, D. A. & Hepler, P. K. (1986) *Protoplasma* **131,** 153–165.
8. Tiwari, S. C., Wick, S. M., Williamson, R. E. & Gunning, B. E. S. (1984) *J. Cell Biol.* **99,** 63s–69s.
9. Cyr, R. J. & Palevitz, B. A. (1989) *Planta* **177,** 245–260.
10. Vantard, M., Schellenbaum, P., Fellous, A. & Lambert, A.-M. (1991) *Biochemistry* **30,** 9334–9340.
11. Jiang, C.-J., Sonobe, S. & Shibaoka, H. (1992) *Plant Cell Physiol.* **33,** 497–501.
12. Jiang, C.-J. & Sonobe, S. (1993) *J. Cell Sci.* **105,** 891–901.
13. Chan, J., Rutten, T. & Lloyd, C. W. (1996) *Plant J.* **10,** 251–259.
14. Lloyd, C. W., Slabas, A. R., Powell, A. J., Macdonald, G. & Badley, R. A. (1979) *Nature (London)* **279,** 239–241.
15. Hussey, P. J., Traas, J. A., Gull, K. & Lloyd, C. W. (1987) *J. Cell Sci.* **88,** 225–230.
16. Xu, P., Lloyd, C. W., Staiger, C. J. & Drobak, B. K. (1992) *Plant Cell* **4,** 941–951.
17. Shelanski, M. L., Gaskin, F. & Cantor, C. R. (1973) *Proc. Natl. Acad. Sci. USA* **70,** 765–768.
18. Hyman, A., Drechsel, D., Kellogg, D., Salser, S., Sawin, K., Steffen, P., 18. Wordemann, L. & Mitchison, T. (1991) *Methods Enzymol.* **196,** 478–485.
19. Jensen, C. G. & Smaill, B. H. (1986) *J. Cell Biol.* **103,** 559–569.
20. Amos, L. A. (1977) *J. Cell Biol.* **72,** 642–654.
21. Jensen, C. G., Bollard, S. M., L. C. W. Jensen, J. L. & Bowser, S. S. (1990) *J. Ultrastruct. Res.* **105,** 1–10.
22. Andreu, J. M., Bordas, J., Diaz, J. F., Garcia de Ancos, J., Medrano, G. R., Nogales, E., Pantos, E. & Towns-Andrews, E. (1992) *J. Mol. Biol.* **226,** 169–184.
23. Jensen, C. G., Bollard, S. M. & Roos, U. P. (1991) *Eur. J. Cell Biol.* **54,** 121–131.
24. Rutten, T., Chan, J. & Lloyd, C. W. (1997) *Proc. Natl. Acad. Sci. USA* **94,** 4469–4474.
25. Scott, C. W., Klika, A. B., Lo, M. M. S., Norris, T. E. & Caputo, C. B. (1992) *J. Neurosci. Res.* **33,** 19–29.
26. Durso, N. A., Leslie, J. D. & Cyr, R. J. (1996) *Protoplasma* **190,** 141–150.
27. Bokros, C. L., Hugdahl, J. D., Kim, H.-H., Hanesworth, V. R., van Heerden, A., Browning, K. S. & Morejohn, L. C. (1995) *Proc. Natl. Acad. Sci. USA* **92,** 7120–7124.
28. Gustke, N., Trinzek, B., Biernat, J., Mandelkow, E.-M. & Mandelkow, E. (1994) *Biochemistry* **33,** 9511–9522.
29. Lewis, S. A., Ivanov, I. E., Lee, G.-H. & Cowan, N. J. (1989) *Nature (London)* **342,** 498–504.
30. Weisshaar, B., Doll, T. & Matus, A. (1992) *Development (Cambridge, U.K.)* **116,** 1151–1161.
31. Chapin, S. J., Bulinski, J. C. & Gundersen, G. G. (1991) *Nature (London)* **349,** 24.
32. Ledbetter, M. C. & Porter, K. R. (1964) *Science* **144,** 872–874.
33. Amos, L. (1995) *Trends Cell Biol.* **5,** 48–51.
34. Cretien, D., Flyvbjerg, H. & Fuller, S. D. (1998) *Eur. Biophys. J.* **27,** 490–500.
35. Mandelkow, E., Song, Y.-H. & Mandelkow, E.-M. (1995) *Trends Cell Biol.* **5,** 262–266.
36. Yuan, M., Shaw, P. J., Warn, R. M. & Lloyd, C. W. (1994) *Proc. Natl. Acad. Sci. USA* **91,** 6050–6053.
37. Mueller, S. C. & Brown, R. M. (1980) *J. Cell Biol.* **84,** 315–326.